Supplementary Materials for Intrinsic and apparent slip at gas-enriched liquid-liquid interfaces: A molecular dynamics study

Emanuele Telari, Antonio Tinti, and Alberto Giacomello

Dipartimento di Ingegneria Meccanica e Aerospaziale, Sapienza Università di Roma, Via Eudossiana 18, 00184 Rome, Italy

Contents

1 Analytical Results

1.1 LIS System

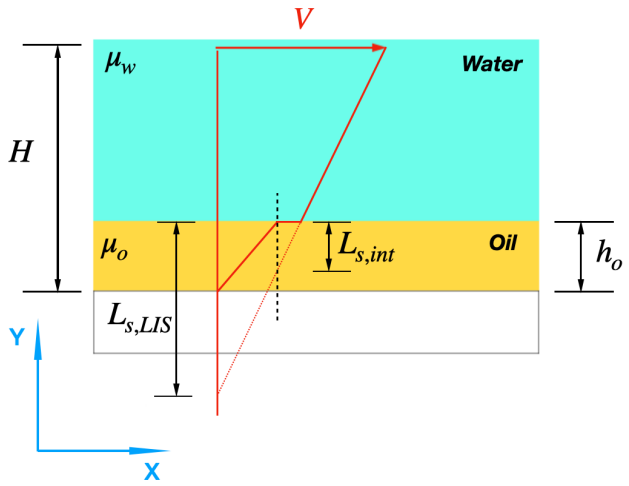

Figure S1: Sketch of the system. H stands for the height of channel at which the shearing velocity V is imposed.$L_{s,LIS}$ is the total slip length measured at the surface containg the contributes of $L_{s,ow}$, the slip length given by the interposition of the oil slab, and $L_{s,int}$ the slip length at the oil-water interface.

Here we report a sketch of the analytical calculations for a Couette two-phase shear flow at a wall (Fig. S1). These calculations easily allow to express the contribution of the liquid-liquid interface slip $L_{s,int}$ to the effective slip length $L_{s,LIS}$ of a LIS. In the absence of slip at the oil-water interface, $L_{s,LIS}$ is related to the viscosity ratio of the two liquids $\gamma = \mu_w/\mu_o$ and to the oil slab height h_o through:

$$L_{s,LIS} = L_{s,ow} = \gamma h_o$$

A general Couette flow, possibly including liquid-liquid slip, is characterized by piecewise linear velocity profiles, thus

$$\begin{aligned} \text{Velocity in oil:} \quad & v_o(y) = Ay + B \\ \text{Velocity in water:} \quad & v_w(y) = C(y - h_o) + D \end{aligned}$$

with the boundary conditions:

$$\begin{aligned} \text{No slip at the solid walls:} \quad & v_o(0) = 0, v_w(H) = V \\ \text{Slip condition at oil-water interface:} \quad & v_w(h_o) - v_o(h_o) = L_{s,int}\frac{\partial v_w(h_o)}{\partial y} \\ \text{Stress continuity at the interface:} \quad & \mu_w\frac{\partial v_w(h_o)}{\partial y} = \mu_o\frac{\partial v_o(h_o)}{\partial y} \end{aligned}$$

With these positions, it is possible to derive the coefficients A, B, C and D.

By defining :

$$\alpha = C = \frac{V}{H + L_{s,int} + h_o\left(\frac{\mu_w}{\mu_o} - 1\right)}$$

we can express the velocity profiles as:

$$v_w(y) = \gamma\alpha y$$

$$v_o(y) = \alpha(y - h_o) + (L_{s,int} + \gamma h_o)\alpha$$

The effective slip length now reads:

$$L_{s,LIS} = v_w(h_o)/\frac{\partial v_w(h_o)}{\partial y} = L_{s,int} + \gamma h_o \tag{1}$$

1.2 Triphase Model

Here we reported the analytical solution for a system (Fig. S2) composed by two liquid phases with a gaseous phase interposed between them. The purpose is to find a relation between the slip length L_s and the viscosity ratio of the liquid and gaseous phases. The system correspond to a zoom of the previous system on the interface region in the case in which a fully developed layer of gas is present between the two liquids. L_s corresponds to the quantity previously called $L_{s,int}$. For simplicity and similarity with the systems we simulated, the two liquid phases are supposed identical, not taking into account the difference in the viscosities between water and oil.
In the same way we did for the previous system, we define:

$$\begin{aligned}
\text{Velocity profile for liquid 1:} \quad & v_1(y) = A(y + \frac{D}{2}) + B \\
\text{Velocity profile in the gas slab:} \quad & v_g(y) = C(y + \frac{w}{2}) + D \\
\text{Velocity profile for liquid 2:} \quad & v_2(y) = E(y - \frac{w}{2}) + F
\end{aligned}$$

The boundary conditions:

- No slip at all interfaces:

$$v_1(-\frac{D}{2}) = 0$$

$$v_1(-\frac{w}{2}) = v_g(-\frac{w}{2})$$

$$v_g(\frac{w}{2}) = v_2(\frac{w}{2})$$

$$v_2(\frac{D}{2}) = V$$

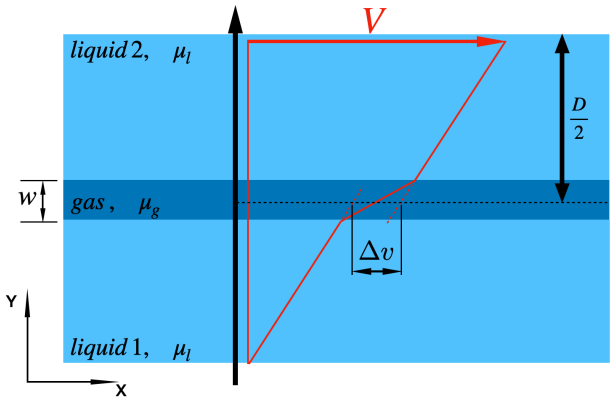

Figure S2: Sketch of the three fluids system.

- Continuity of stress:

$$\mu_l \frac{\partial v_1(-\frac{w}{2})}{\partial y} = \mu_g \frac{\partial v_g(-\frac{w}{2})}{\partial y}$$

$$\mu_g \frac{\partial v_g(\frac{w}{2})}{\partial y} = \mu_l \frac{\partial v_2(\frac{w}{2})}{\partial y}$$

allow to derive the relation:

$$L_s = (\gamma - 1)w, \quad \gamma = \frac{\mu_l}{\mu_g} \tag{2}$$

for the apparent slip length.

2 Simulation Details

2.1 Molecular Dynamics

Shear simulations were carried out for $11 \cdot 10^6$ timesteps, with $\Delta t = 0.003\tau$; we discarded the first $3 \cdot 10^6$ timesteps and collected statistics in the remaining ones, printing data every 1000 steps. The data collected were divided into 10 subsets and the average values and the uncertainty have been obtained from a block averaging procedure [Janke(2002)].

Pressure control was achieved by mechanically forcing the upper wall in the direction orthogonal to the liquid-liquid interface. In order to ensure rigidity of the moving wall at each integration timestep, forces on the wall atoms are first individually computed according to the interatomic interactions, then averaged so that each wall atom experiences the same average force; finally a given constant force is added to each atom resulting in the desired pressure (this is implemented in the "`fix aveforce`" command in LAMMPS).

2.2 Validation of the simulation protocol

Prior to the adoption of the computational strategy described in the earlier sections and in the main text several simulation protocols were evaluated. In particular we made sure that that the thermostat is able to provide precise temperature control while not dramatically influencing the velocity profile induced by the shear. This is a crucial point in order to obtain reliable estimates of L_s and to make sure that the measures for the different systems (e.g. at varying gas concentrations) are consistent to each other.

Our investigation started by considering a simple biphase system, periodic in the three spatial dimensions. Lees and Edwards boundary conditions[Evans & Morriss(2001), Lees & Edwards(1972)] were employed in order to induce a shear flow, while the two liquids were kept at constant temperature by a Nosé-Hoover chains (NHC) thermostat with a chain length of four and a dampening parameter of 100 timesteps. In this regard two different thermostating protocols were employed; In the first one the thermostat only acts on the degrees of freedom that are orthogonal to the shear flow, i.e. in the X and Z directions, whereas, acccording to the second protocol, the thermostat is set free to control all components of the velocity but only after subtracting, at each step, the velocity profile induced by the shear (For more information on such protocols we refer to [Evans & Morriss(2001)]). The results shown in Fig. S3 display a good agreement between the velocity profiles obtained using the two protocols.

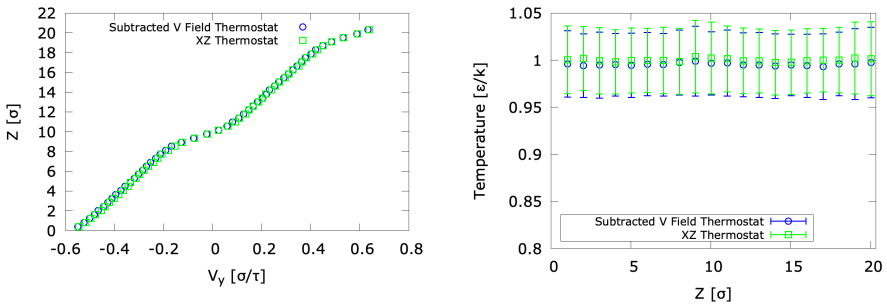

(a) (b)

Figure S3: *a*) Comparison between the two velocity profiles obtained using the thermostat acting on only X and Z degrees of freedom (green squares) and the thermostat controlling the velocities after subtracting an average velocity profile at each simulation step (blue circles). *b*) Comparison between the temperature profiles obtained using the two thermostats, symbols as in figure (a).

Early simulations, making use the Lees and Edwards boundary conditions to induce shear, indicated the need for a reliable strategy to control the pressure in the system, in order to obtain comparable results at various gas concentrations.

For this reason we decided to adopt a non periodic system enclosed by rigid

walls as a means of inducing the shear flow. In this protocol the bottom wall remains motionless, while the upper wall moves with prescribed velocity in the flow direction, while being free to move in the direction orthogonal to the wall itself. A constant force is then applied in the orthogonal direction in order to mechanically induce pressure control. Using this simple mechanical route the pressure of the system was reliably fixed at $0.4\frac{\varepsilon}{\sigma^3}$ irrespective of the composition of the fluid. A NHC thermostat with $N_{chain} = 4$ and a damping parameter of 100 timesteps is used to control the temperature of the fluid, by controlling velocity components that are orthogonal to the shear flow.

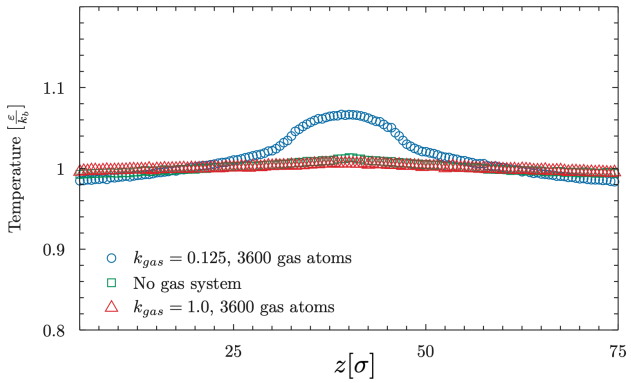

Figure S4: Temperature profiles for three fluid compositions: no gas atoms (green squares), 3600 $k_{gas} = 1.0$ gas atoms (red triangles) and and 3600 $k_{gas} = 0.125$ gas atoms (blue circles). A negligible increase of the temperature is found in the interfacial region, for the first two systems. In the last case, the temperature increase is more significant, reaching about 6% of the reference value.

The temperature profiles (as extracted from the fluid velocity components that are orthogonal the shear flow) for the final system are shown in Fig. S4 for two extreme cases in terms of concentration of the gas atoms and two values of $k_{gas} = 0.125$,$k_{gas} = 1.0$. The temperature profiles exhibited by the systems are flat, with slight deviations due to increased heat production in the central region. As expected the increase in temperature, while not dramatic, is more evident for the realizations associated to large slip and is inherent in the dynamics of the interface under shear, reaching a maximum local increase of about 6%. In conclusion the temperature deviations in the central region, as be observed via close inspection of the temperature profiles, can be considered minimal and do not induce large changes in the properties of the fluids, including the velocity profiles and slip properties.

As a further validation of the thermostating protocol Fig. S5 proposes a comparison of the slip lengths observed, as a function of the number of third species atoms, as obtained using the early Lees and Edwards protocol and the final production runs with full pressure control. Absolute results differ due to

the dramatically different thermodynamical conditions that are portrayed in the two sets of simulations, yet the trends observed remain valid in the two cases.

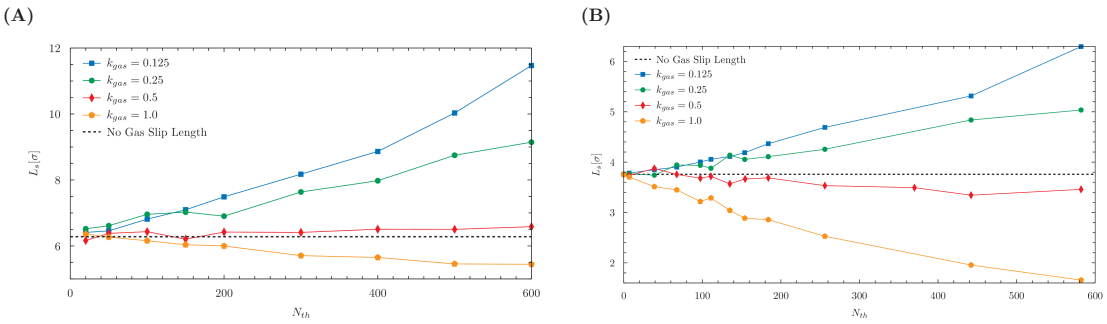

Figure S5: Comparison between results obtained in the non periodic (A) and in the periodic systems (B). Trends are comparable, but absolute values are different due to the higher pressures in the non periodic system.

2.3 Linear Response Regime

As customary in MD simulations of slip, our simulations are computed at relatively large shear rates in order to maintain an acceptable signal to noise ratio. For this reason it was extremely important for us to ensure that our system is in the linear response regime, i. e., ensuring that the slip length does not depend on the imposed shear rate.

In order provide proof that the simulations object of the present work are indeed in the linear response regime, we performed simulations at different sliding velocities of the wall, for a two liquids system. Results are shown in Fig. S6.

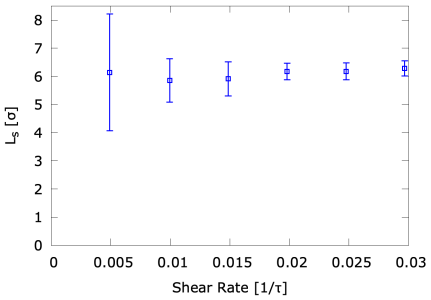

Figure S6: Dependence of the slip length value on the shear rate. The last point of the graph correspond to the highest shear rate experienced in our systems.

We also take to opportunity to recall how, as mechanical pressure control inherently induces small vertical displacements of the walls, whose velocity is

kept fixed, there will be slight differences in the shear rates among the various systems object of our investigation characterized by different values of N_{th}.

2.4 Size of the System

The distance between the two walls has been carefully verified to be appropriate such that the walls, needed to control the pressure and apply shear, have no influence on the interface phenomena we aimed to study. This has been carefully verified by checking the density oscillations due to the layering of the liquid (Fig. S7). For the same reason, the interactions between walls and third species have been set to be purely repulsive which avoids unwanted gas accumulation at the walls.

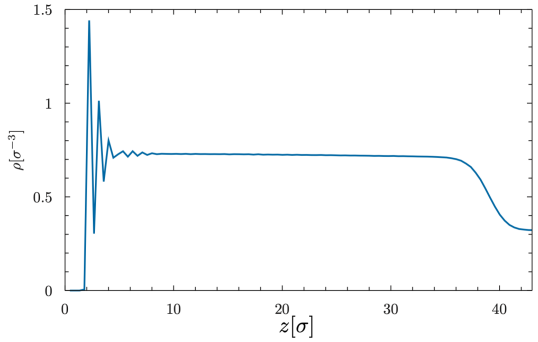

Figure S7: Total density profile in the region ranging from the bottom wall to the liquid-liquid interface.

2.5 Calculations of Solubility from Simulations

Calculations for the solubility were carried out for six different values of k_{gas}, corresponding to six different liquid-third species interactions. The systems simulated comprised 32000 liquid atoms in a cubic box of dimensions $35.45\sigma \times 35.45\sigma \times 35.45\sigma$ at prescribed temperature and density ($T = 1$, $\rho = 0.718$). Simulations in the NVT ensemble were performed using a Nosé-Hoover chains thermostat with a chain length of three and a dampening parameter of 100 timesteps, with a timestep $\Delta t = 0.005\tau$. The liquid-liquid interaction parameters were set to $\varepsilon_{11} = 1$ and $\sigma_{11} = 1$.

The solvation free-energy was computed via thermodynamic integration [Kirkwood(1935), Frenkel & Smit(2001)] by using a soft L-J potential $U_{soft}(\lambda)$ to model the solute-solvent interaction. The soft L-J potential has the functional form

$$U_{soft}(\lambda) = \sum_{atoms} 4\varepsilon\lambda^n \left(\frac{1}{(\alpha(1-\lambda)^2 + (\frac{r}{s})^6)^2} - \frac{1}{\alpha(1-\lambda)^2 + (\frac{r}{s})^6} \right) \qquad (3)$$

with $\alpha = 0.5$ and $n = 2$ and a cutoff at $r_{cut} = 3.5\sigma$ which was not indicated in the functional form for simplicity. The soft potential allows to continuously and smoothly interpolate between the case $\lambda = 0$ (i.e. no solvent particle is present) to the case $\lambda = 1$ which exactly reproduces the desired L-J interaction with the solute particle, enabling the calculation of free energies via thermodynamic integration. This special functional form for the soft potential was proposed by [Beutler et al. (1994)] and it is by now a standard tool in thermodynamic integration calculations to avoid discontinuities associated with the creation/annihilation of the solute atom.

The solvation free energy can now be expressed as the definite integral with respect to λ over the interval $\lambda \in [0, 1]$ of the ensemble average of the derivative of the potential energy of the system $U = U_{soft} + U_{liq-liq}$ with respect to λ:

$$\Delta G_{solv} = \int_0^1 \left\langle \frac{\partial U}{\partial \lambda} \right\rangle d\lambda \ . \tag{4}$$

The quantity $\left\langle \frac{\partial U}{\partial \lambda} \right\rangle$ was then computed, for several values of λ from the radial distribution functions $g(r)$ of the liquid with respect to the solute particle via

$$\left\langle \frac{\partial U}{\partial \lambda} \right\rangle = 4\pi\rho \int_0^\infty \frac{\partial U_{soft}}{\partial \lambda} g(r) r^2 \, dr \ . \tag{5}$$

For every value of k_{gas}, in order to carry out the integration in Eq. (4), 32 values of the λ parameter, uniformly distributed in the interval $[0, 1]$ were considered; Each of these simulations was carried out for $1.5 \cdot 10^6$ timesteps (timestep=0.005 τ) of which the last $1 \cdot 10^6$ were used to compute radial distribution functions.

2.6 Theoretial estimates for the solubility

We refer to the theory in [Reiss et al.(1960), Wilhelm & Battino (1971)], where the total solvation energy is expressed as:

$$\Delta G_{solv} = \Delta G_c + \Delta G_i \tag{6}$$

with the two terms on the RHS being the partial Gibbs free energy of cavity formation and of interaction with the liquid, respectively. These the two terms can be expressed as:

$$\Delta G_c = k_B T \left\{ 6\frac{y}{1-y}\left[2\left(\frac{\sigma_{12}}{\sigma_1}\right)^2 - \frac{\sigma_{12}}{\sigma_1}\right] + 18\left(\frac{y}{1-y}\right)^2 \left[\left(\frac{\sigma_{12}}{\sigma_1}\right)^2 - \frac{\sigma_{12}}{\sigma_1} + \frac{1}{4}\right] - \ln(1-y) \right\} \tag{7}$$

with

$$y = \pi\sigma_1\rho/6$$

and

$$\Delta G_i = -3.555\pi\rho\sigma_{12}\varepsilon_{12} \ , \tag{8}$$

where σ_1 and σ_{12} correspond to the σ parameters of the L-J potential for the liquid-liquid interactions and the inserted particle-liquid interactions, respectively, ρ is the bulk density, T is the temperature, k_B the Boltzmann constant, and ε_{12} is the energy parameter of the inserted particle-liquid interactions.
In our case, all the σ parameters are fixed; the only changing parameter is ε_{12}, so our ΔG_{solv} must show a linear behaviour of the type:

$$\Delta G_{solv} = A + B\varepsilon_{12} \tag{9}$$

where, in our case, $\varepsilon_{12} = k_{gas}\varepsilon_{11}$ and $\varepsilon_{11} = 1$, yielding the theoretical estimate:

$$A = \Delta G_c \qquad B = -3.555\pi\rho\sigma_{12} \tag{10}$$

3 Viscosities

3.1 Non-equilibrium Calculation of the Viscosities

Viscosity profiles have been calculated using the relation:

$$\mu = \frac{\tau_{xz}}{\frac{\partial v}{\partial z}} \ . \tag{11}$$

The shear stress τ_{xz} was obtained by averaging over the shear stress profile obtained dividing the simulation box in slabs, with a procedure reminiscent to the one carried out for the reconstruction of the velocity profile. Subsequently, τ_{xz} was divided by the local derivative of the velocity profile $\frac{\partial V}{\partial Z}$ in order to obtain the viscosity profile. In order to estimate the liquid bulk, μ_{bulk}, and interface, μ_{int}, viscosities, the profile was averaged over the bulk region and the interface region defined by L_{int}, respectively. In Fig. S8 we report the results for μ_{int} and for the viscosity ratio $\gamma = \frac{\mu_{bulk}}{\mu_{int}}$ for the systems where the gas layer formed, and compared them to the value expected from the Green-Kubo calculations (see below). The results exhibit good agreements, in particular as the gas layer thickens its visosity tends to the values obtained (for a bulk system) using Green-Kubo formalism (see Sec. 3.2).

3.2 Viscosities from Green-Kubo Calculations

Long equilibrium simulations ($6 \cdot 10^7$ MD steps) were used to compute bulk viscosities from stress autocorrelations using the Green-Kubo formalism. These simulations were performed in the canonical ensemble using a Langevin thermostat by matching the densities of the equilibrium case during equilibration and then integrating at constant energy (NVE ensemble) during the production runs, while using the very same truncated and shifted L-J interatomic potentials that were used in the NEMD simulations. The size of the box was set to $8192\sigma^3$. Initially the system was evolved in the NVT ensemble (using a Langevin thermostat damping parameter set to 1τ with an elementary timestep of 0.005τ) until equilibration, after which the production phase was conducted

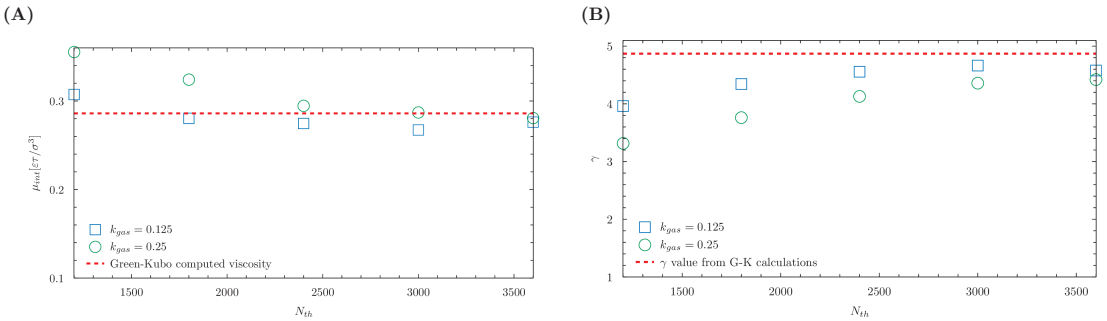

Figure S8: *A*) Values of the interface viscosity μ_{int} obtained by the viscosity profiles for the systems in the interposed gas layer regime. Red dashed line stands for the value of viscosity calculated with Green-Kubo calculations for a bulk of the interposed layer phase. *B*) Values of the viscosity ratios γ for the systems in the interposed gas layer regime. Red dashed line stands for the value of the ratio of the viscosities μ_{bulk} and μ_{int} obtained from the Green-Kubo calculations

resorting to NVE dynamics. In particular the case for a pure liquid was equilibrated at density $\rho = 0.718$ and $T = 1.0\varepsilon/k_B$, $6 \cdot 10^7$ simulation steps were performed. Correlations were computed after discarding the first $1 \cdot 10^7$ steps yielding a value of $1.395\varepsilon\tau/\sigma^3$ which is compatible with similar results obtained by [Galliero et al. (2005)].

Similarly, we computed viscosity for a solution with the exact densities for the various species as found in the gas slab, namely $\rho_1 = \rho_2 = 0.032$ and $\rho_3 = 0.25$, with $k_{gas} = 0.125$. This simulation resulted in a value of $0.286\varepsilon\tau/\sigma^3$ for the viscosity of the mixture. We also conducted a measurement at the temperature $T = 1.06\varepsilon/k_B$ in order to gauge the effect of the slight temperature increase introduced by the shearing at the very center of the gas slab. Using the compositions $\rho_1 = \rho_2 = 0.042$ and $\rho_3 = 0.23$, and sampling for $1 \cdot 10^6$ MD steps we obtained a value for the viscosity of $0.272\varepsilon\tau/\sigma^3$, displaying minimal deviations from the $T = 1.00$ results.

4 Radial Distribution Functions

For the above mentioned mixture ($\rho_1 = \rho_2 = 0.032$ and $\rho_3 = 0.25$, with $k_{gas} = 0.125$) we also measured radial density functions for various combinations of species. From the profiles extremely limited oscillations can be observed just above the soft repulsion distance.

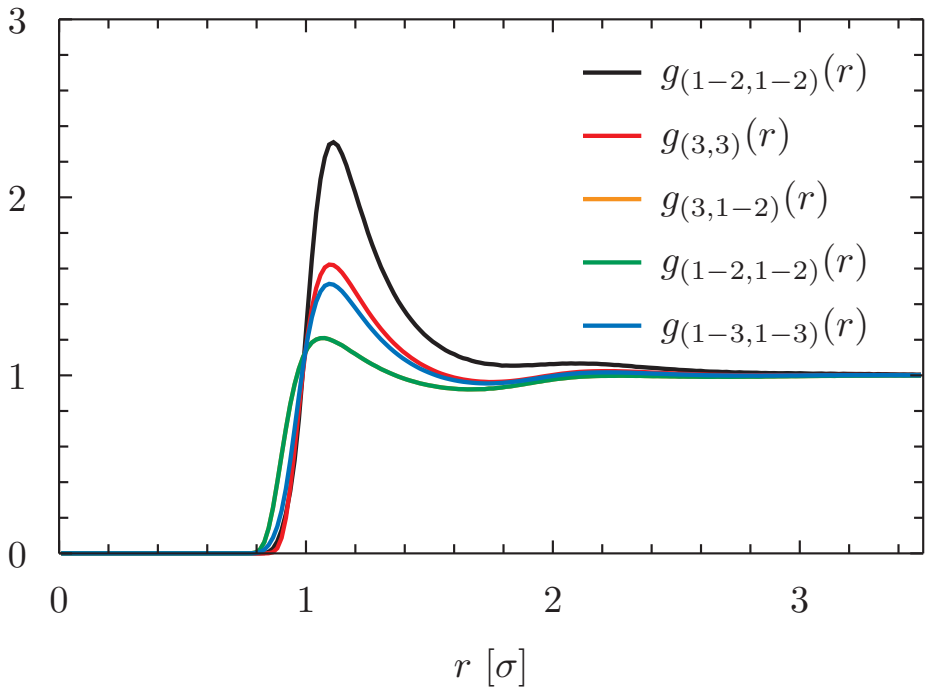

Figure S9: Radial density calculations for the mixture $\rho_{liq1} = \rho_{liq2} = 0.032$ and $\rho_{th} = 0.25$, with $k_{gas} = 0.125$).

5 Stability of the gas layer

5.1 Influence of shear on the fluid density profiles

By simulating the system in static conditions (i.e. without any shear) it is possible to demonstrate how the shear has no influence on the gas density profiles, with the third species accumulating at the liquid-liquid interface in both cases. This finding suggests that the interface structure mainly depends on the static interaction between the two fluids resulting in a depleted region at the interface that is preferentially enriched by atoms of the poorly soluble species. This scenario holds also in presence of a fully developed gas layer (Fig. S10), although the slight increase in temperature due to shear is able to slightly modify the bulk density of the central region (See .Fig. S11).

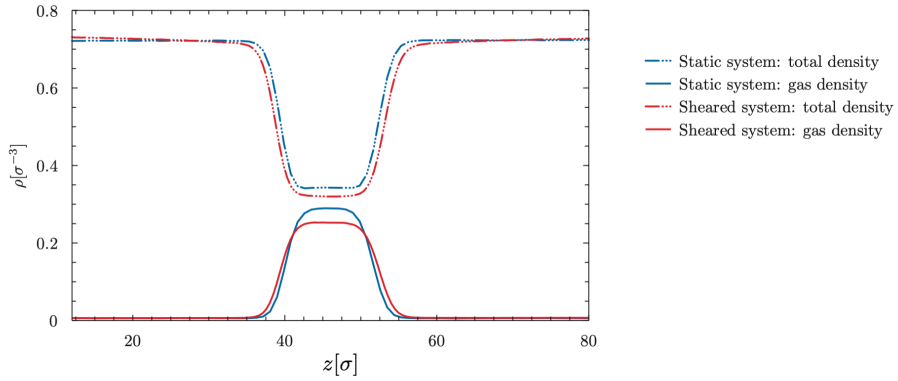

Figure S10: Gas and total density profiles for the system with $k_{gas} = 0.125$ and 3000 gas atoms in static conditions and under shear.

5.2 Stability of the gas layer with respect to pressure increase

The gas layer interposed between the liquids was found to be very stable with respect to pressure variations: increased pressure conditions do not seem to preclude the formation of a stable gas layer, which was observed also at the highest simulated pressures of $0.8\varepsilon/\sigma^3$. (Fig. S12).

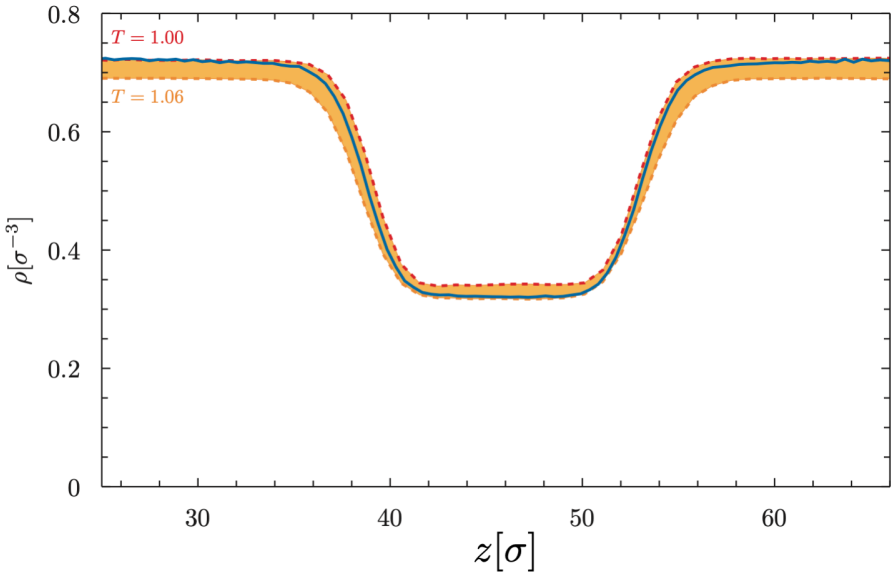

Figure S11: Average total density profile of the sheared system (blue line) with 3000 gas atoms and $k_{gas} = 0.125$ as compared to the total density profiles for the static systems at $T = 1$ (dashed red line) and $T = 1.06$ (dashed orange line) in the region close to the slab. The region between the two static density profiles is shaded.

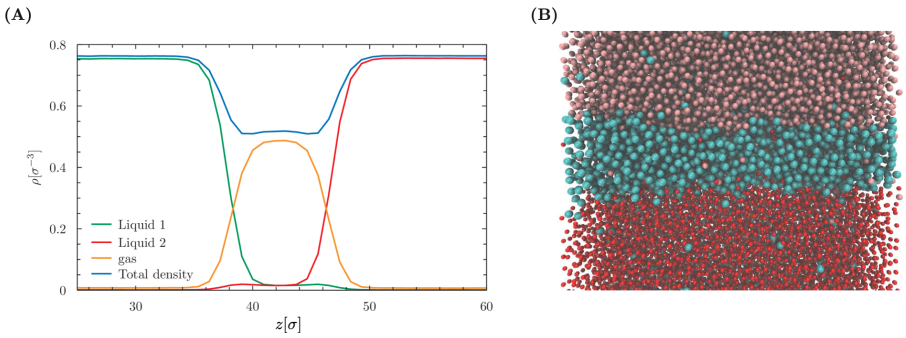

Figure S12: (A): Average density profiles for the 36000 atoms and $k_{gas} = 0.125$ system in static conditions at a large pressure of about $0.8\varepsilon/\sigma^3$ (i.e. twice the $0.4\varepsilon/\sigma^3$ pressure imposed in the shear simulations). (B): snapshot of the interface.

References

[Beutler et al. (1994)] Beutler, T. C., Mark, A. E., van Schaik, R. C., Gerber, P. R., & van Gunsteren, W. F. (1994). Avoiding singularities and numerical instabilities in free energy calculations based on molecular simulations. *Chem. Phys. Lett.*, *222*, 6.

[Evans & Morriss(2001)] Evans, D. J., & Morriss, G. P. (1986). Shear thickening and turbulence in simple fluids. *Phys. Rev. Lett.*, *56*, 2172-2175 (1986).

[Lees & Edwards(1972)] Lees, A. W., Edwards, S. F. (1972). The computer study of transport processes under extreme conditions. *J. Phys. C: Solid State Phys.*, *5*, 1921

[Frenkel & Smit(2001)] Frenkel, D. & Berend, S. (2001). Understanding molecular simulation: from algorithms to applications. *Elsevier*

[Galliero et al. (2005)] Galliéro, G. and Boned, C. and Baylaucq, A. (2005). Molecular Dynamics Study of the Lennard-Jones Fluid Viscosity: Application to Real Fluids *Ind. Eng. Chem. Res.*, *(44)17* 6963–6972

[Janke(2002)] Janke, W. (2002). Statistical analysis of simulations: Data correlations and error estimation. In *Quantum Simulations of Complex Many-Body Systems: From Theory to Algorithms*, J. Grotendorst, D. Marx, A. Muramatsu (Eds.), John von Neumann Institute for Computing, Jülich, *10*, 423-445.

[Kirkwood(1935)] Kirkwood, J. G. (1935). Statistical Mechanics of Fluid Mixtures. *Journal of Chemical Physics*, *3*, 300-313.

[Reiss et al.(1960)] Reiss, H., Frisch, H. L., Helfand, E., & Lebowitz, J. L. (1960). Aspects of the statistical thermodynamics of real fluids. *J. Chem. Phys.*, *32*(1), 119-124.

[Wilhelm & Battino (1971)] Wilhelm, E., & Battino, R. (1971). Estimation of Lennard-Jones (6,12) Pair Potential Parameters from Gas Solubility Data. *J. Chem. Phys.*, *55*, 4012.